

Cross Sections of Solar Neutrino Capture by ^{127}I Nuclei and Gamow–Teller Resonances

Yu. S. Lutostansky^{1,*}, A. N. Fazliakhmetov^{1,2,3}, G. A.
Koroteev^{1,2,**}, N. V. Klochkova¹, A. P. Osipenko¹, and V. N.
Tikhonov¹

¹*National Research Centre "Kurchatov Institute", Moscow, Russia*

²*Moscow Institute of Physics and Technology, Dolgoprudny, Russia*

³*Institute for Nuclear Research of Russian Academy of Sciences,
Moscow, Russia*

E-mail:

* *lutostansky@yandex.ru*

** *koroteev@phystech.edu*

March 24, 2021

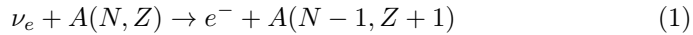
Abstract

Solar neutrino capture cross-section $\sigma(E)$ by ^{127}I nucleus has been studied with taking into account the influence of the resonance structure of the nuclear strength function $S(E)$. Three types of isobaric resonances: giant Gamow-Teller, analog resonance and low-lying Gamow-Teller pigmy resonances has been investigated on the framework of self-consistent theory of finite Fermi systems. The calculations have been performed considering the resonance structure of the charge-exchange strength function $S(E)$. We analyze the effect of each resonance on the energy dependence of $\sigma(E)$. It has been shown that all high-lying resonances should be considered in the $\sigma(E)$ estimations. Neutron emission process for high energy nuclear excitation leads to formation ^{126}Xe isotope. We evaluate contribution from various sources of solar neutrinos to the $\sigma(E)$ structure and to the $^{126}\text{Xe}/^{127}\text{Xe}$ isotopes ratio formed by energetic neutrinos. $^{126}\text{Xe}/^{127}\text{Xe}$ isotope ratio could be an indicator of high-energy *boron* neutrinos in the solar spectrum. We also discuss the uncertainties in the often used Fermi-functions calculations.

1 Introduction

In neutrino physics and astrophysics, the process of interaction of neutrino with matter is of great importance. In most cases, it is needed to calculate neutrino capture cross-section $\sigma(E)$ and take into account the structure of the

charge-exchange strength function $S(E)$, which determines the magnitude of $\sigma(E)$ and its energy dependence. The charge-exchange strength function $S(E)$ has a resonant nature, and its structure affects the neutrino capture cross-section $\sigma(E)$. This is particularly important for the simulation of neutrino detectors based on the ν -capture reaction



The first proposed isotope for the neutrino detection was ^{37}Cl . The chlorine–argon radiochemical method was proposed by Pontecorvo in 1946 [1] and later implemented by Davis [2] in the United States. Implementation of the gallium–germanium method for measuring solar neutrinos was started after [3], [4] papers. A low-threshold detector for the $^{71}\text{Ga}(\nu_e, e^-)^{71}\text{Ge}$ reaction was established at an underground laboratory and was well protected from cosmic rays (for more details, see review [5]).

Another approach of neutrino detection is iodine-xenon reaction based radiochemical method



with the threshold of $Q = 662.3 \pm 0.20$ keV lower than the ^{37}Cl one ($Q = 813.87 \pm 0.20$ keV [6]), which increases the neutrino capture cross-section $\sigma(E)$. Such detector can detect not only ^8B solar neutrinos but also ^7Be ones. In 1988, Haxton [7] pointed out that the cross-section $\sigma(E)$ for the reaction (2) on iodine could be much larger than that on ^{37}Cl and that the detection volume for iodine can be made much larger than the chlorine detector. However, no calculations of the cross-section $\sigma(E)$ for the reaction (2) were performed at that time, only estimations. In the following year, calculations in [8] were performed including the resonance structure of the charge-exchange strength function $S(E)$ of the ^{127}Xe daughter nucleus. In 1991, those calculations were refined in [9] with allowance for special features of the normalization of the strength function $S(E)$, and the *quenching*-effect was taken into account (for more details, see [10]). In the late 90s, there was a proposal to develop solar neutrino detector with ^{127}I as the target in the Homestake laboratory (USA) [11], [12], [13]. Also in Los Alamos National laboratory neutrino capture cross-section with ^{127}I as the target was investigated on the accelerator beam [14]. The strength function $S(E)$ was measured in the $^{127}\text{I}(p, n)^{127}\text{Xe}$ reaction in 1999 [15], and these experimental data appeared to be in good agreement with our predictions made in [8] [9]. The calculations performed at that time by Engel, Pittel, and Vogel [16] [17] are also noteworthy. According to [15], the comparison with the experimental dependence of the strength function $S(E)$ demonstrates that the calculations in [9] have a higher prediction accuracy.

However, previous calculations did not include the possibility of the formation of the stable ^{126}Xe isotope in the neutrino capture reaction (2) in the iodine detector. High-lying charge-exchange resonances in the strength function $S(E)$ determine the formation of the stable ^{126}Xe isotope upon the capture of high energy solar neutrinos by the ^{127}I nucleus and the subsequent emission of a neutron from the formed ^{127}Xe nucleus.

In the resonance structure of the charge-exchange strength function of ^{127}Xe nucleus can be identified three types of isobaric resonances (see Fig. 1): giant Gamov-Teller (GTR), analog (AR), and low-lying Gamov-Teller pigmy resonances (PR) [18]. Similar resonance structure can also be observed in other

neutron-rich nuclei [19]. Recently it was shown [10] [20] [21] that in the calculation of the total neutrino capture cross-section $\sigma(E)$ should take into account all types of resonances. Ignoring even high-lying ones, such as GTR, leads to a deficit in the cross-section $\sigma(E)$, which can significantly affect the interpretation of experimental data. In calculations of $\sigma(E)$ for capture solar neutrinos [21] [22] were obtained similar results demonstrating that it is necessary to include all resonances in the charge-exchange strength function $S(E)$.

2 Excited states structure of the ^{127}Xe nucleus

Fig. 1 shows the scheme of excited states of the ^{127}Xe isobaric nucleus, various regions of the excitation spectrum, and isotopes formed as a result of neutrino capture by the ^{127}I nucleus and subsequent decay. The respective experimental data were obtained in the reaction $^{127}\text{I}(p, n)^{127}\text{Xe}$ [15] and a table of values of matrix elements $B(GT)$ depending on the energy E_x (with 0.5 MeV step) in the daughter nucleus ^{127}Xe up to the energy 20 MeV was presented. It was found that the total sum of $B(GT)$ up to 20 MeV energy is 53.54 ± 0.22 [15], which is $\approx 85\%$ of total GT summ rule $3(N - Z) = 63$ for ^{127}I . Below, we will discuss the reasons behind this underestimation (*quenching-effect*).

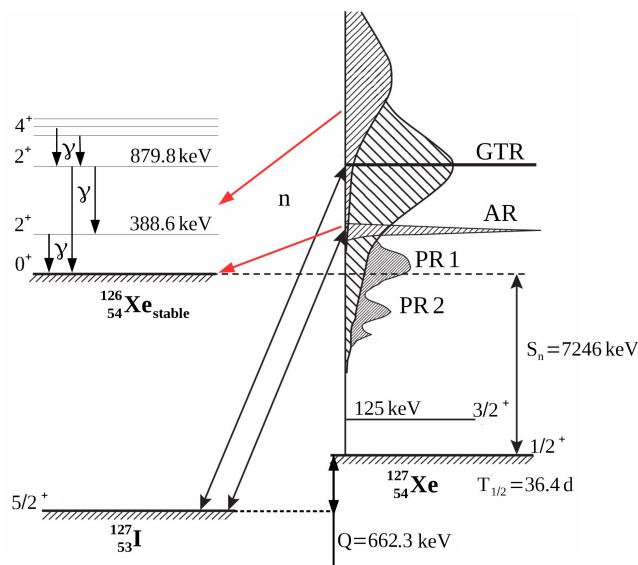


Figure 1: Scheme of charge-exchange excitations of the ^{127}Xe nucleus in the $^{127}\text{I}(p, n)^{127}\text{Xe}$ reaction with the decay of high-lying excitations in the stable ^{126}Xe isotope accompanied by the emission of a neutron. The giant Gamow-Teller resonance (GTR), analog resonance (AR), and lower lying Gamow-Teller pygmy resonances (PR) are indicated; S_n is the neutron separation energy in the ^{127}Xe nucleus

There are also shown in Fig. 1: threshold energy $Q_\beta = 662.3 \pm 2.0$ keV and $S_n = 7246 \pm 5$ keV - neutron separation energy in ^{127}Xe nucleus [23]. Excited states of the ^{127}Xe nucleus at energies above S_n will decay with neutron emission to the stable ^{126}Xe isotope; as a result, neutrino capture on the ^{127}I nucleus in reaction (2) will lead to the formation of the ^{127}Xe and ^{126}Xe isotopes [24]. If the daughter ^{126}Xe nucleus is born on the excited state, the subsequent deexcitation

will lead to the emission of one or several gamma-ray photons. The yield of the stable ^{126}Xe isotope is relatively low, but it survives in the xenon fraction after long-term storage following the decay of the ^{127}Xe ($T_{1/2} = 36.4$ d) isotope. In addition, according to Fig. 1, the production of the ^{126}Xe isotope is accompanied by a transition from the low-lying excited 2^+ state ^{126}Xe to the ground state 0^+ with the emission of gamma-ray photons with the energy $E_1 = 388.6$ keV. Thus, the analysis of the $^{126}\text{Xe}/^{127}\text{Xe}$ isotope ratio in the formed xenon gas mixture and the detection of gamma emission in ^{126}Xe open new capabilities of the iodine detector for the detection of solar neutrinos and make it possible to separate the important boron component of the solar spectrum.

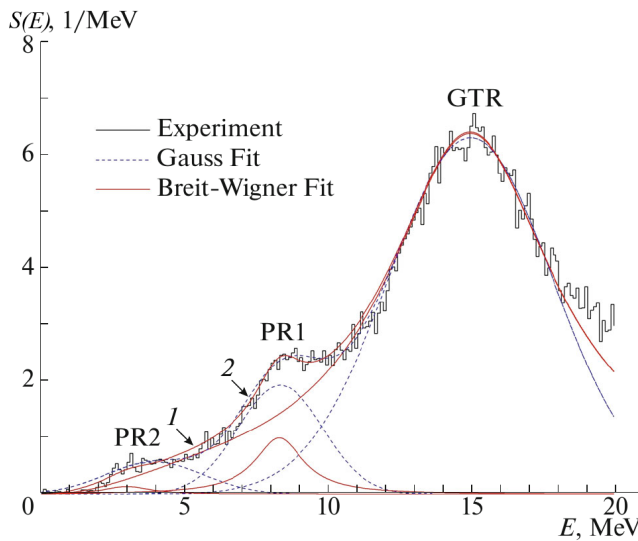


Figure 2: Charge-exchange strength function $S(E)$ distribution for the ^{127}Xe nucleus according to the analysis of $^{127}\text{I}(p, n)^{127}\text{Xe}$ reaction experimental data [15]. Giant Gamow–Teller resonance (GTR) and two pygmy resonances PR1 and PR2 were fitted by Gaussian (G) or by Breit–Wigner (B-W) shape forms. The summed dependencies $S(E) = S(\text{GTR}) + S(\text{PR1}) + S(\text{PR2})$ are given in two approximations: (1) B-W and (2) G.

Fig. 2 represents charge-exchange strength function $S(E)$ for the ^{127}Xe using experimental data analysis of $^{127}\text{I}(p, n)^{127}\text{Xe}$ reaction [15]. $S(E)$ could be submitted as sum of strength functions of three resonances: Giant Gamow–Teller resonance $S(\text{GTR})$ and two pygmy ones $S(\text{PR1})$, $S(\text{PR2})$.

Resonances were fitted by Gaussian (G) or by Breit–Wigner (B-W) shape forms. The summed dependences $S(E) = S(\text{GTR}) + S(\text{PR1}) + S(\text{PR2})$ in the Fig. 2 are given for two approximations: (1) B-W and (2) G.

GTR peak energy $E_{\text{GTR}} = 14.9$ MeV is the same for both fits as well as PR1 peak energy $E_{\text{PR1}} = 8.3$ MeV. Experimental values from [15] are closer to B-W fit results: $E_{\text{GTR}} = 14.5$ MeV, $E_{\text{PR1}} \approx 8.7$ MeV, $E_{\text{PR2}} = 5 - 6$ MeV and $E_{\text{PR3}} = 3.08$ MeV.

3 Strength function calculation

Within the microscopic theory of finite Fermi systems (TFFS), charge-exchange excitations of nuclei are described by the system of equations for the effective

field in the form [25]:

$$V_{pn} = e_q V_{pn}^\omega + \sum_{n'p'} F_{np,n'p'}^\omega \rho_{p'n'}, \quad V_{pn}^h = \sum_{p'n'} F_{np,n'p'}^\omega \rho_{p'n'}^h \quad (3)$$

where V_{pn} and V_{pn}^h are the effective fields of quasiparticles and holes in the nucleus, respectively, and V_{pn}^ω is the external charge-exchange field. The system of secular equations (3) is solved for allowed transitions with a local nucleon–nucleon interaction F_ω in the Landau–Migdal form [25]

$$F_\omega = C_0(f'_0 + g'_0(\vec{\sigma}_1\vec{\sigma}_2))(\vec{\tau}_1\vec{\tau}_2)\delta(\vec{r}_1 - \vec{r}_2) \quad (4)$$

where $C_0 = (d\rho/d\epsilon_F)^{-1} = 300 \text{ MeV}\cdot\text{fm}^3$ (ρ is the average nuclear-matter density) and f'_0 and g'_0 are the parameters of isospin–isospin and spin–isospin quasiparticle interactions, respectively. These coupling constants are phenomenological and could be determined by fitting experimental data.

The inclusion of terms associated with the pion mode leads to an effective renormalization of the coupling constant g'_0 [26]

$$g'_{0eff} = g'_0 - \Delta g'_\pi \quad (5)$$

where $\Delta g'_\pi$ is the correction to g'_0 for the effect of the pion mode associated primarily with a high-lying Δ -isobar. According to the calculations performed in [26] with considering the pion mode, these effects exert an influence on states lying substantially higher than GTR. The values of $f'_0 = 1.35$ and $g'_0 = 1.22$ were obtained earlier in [26] from a comparison of the calculated and measured values of the GTR and AR energies. However, the recent analysis [27] of calculated and experimental data on the energies of analog (for 38 nuclei) and Gamow–Teller (for 20 nuclei) resonances showed that the local-interaction parameters should be slightly corrected [27]:

$$f'_0 = 1.351 \pm 0.027, \quad g'_0 = 1.214 \pm 0.048 \quad (6)$$

The calculations of charge-exchange excitations for the ^{127}I isotope were performed with the inclusion of this correction. The energies, E_i , and the squares of the matrix elements, M_i^2 formed by allowed transitions for excited isobaric states of the ^{127}Xe daughter nucleus were calculated. The matrix elements are normalized according to the sum rule for GT transitions as in [9]:

$$\sum M_i^2 = q[3(N - Z)] = e_q^2[3(N - Z)] \approx \int_0^{E_{max}} S(E)dE = I(E_{max}) \quad (7)$$

where $q < 1$ is the parameter determining the *quenching*-effect (deficit in the sum rule to the maximum theoretical value $3(N - Z)$ at $q = 1$ [28]). Within the TFFS framework, $q = e_q^2$, where e_q is the effective charge [25]; $S(E)$ is the charge-exchange strength function and E_{max} is the maximum energy taken into account in the calculations or in the experiment. In the present calculations we used the value $E_{max} = 20 \text{ MeV}$, as in the experiment reported in [15]. The value $q = 0.85$ was obtained in [15] for ^{127}I , which is close to the calculated one. Should be noted that for other nuclei, the calculated values of e_q differ from 0.9, mainly to a lower side [10] [21]. In experiments, the sum in Eq. (7) rarely reaches

$q = 0.70$ (70%) of $3(N - Z)$, primarily because of moderately small values of the energy E_{max} , difficulties encountered in separating and subtracting backgrounds at energies above E_{GTR} as well as the result of two-particle-two-hole excitations or Δ -isobar-neutron-hole excitation.

Since the spectrum of the function $S(E)$ has a continuous resonance structure, the Breit-Wigner form was chosen for partial amplitudes $S_i(E)$:

$$S_i(E) = M_i^2 \frac{\Gamma_i}{(E - E_i)^2 + \Gamma_i^2} \phi(E) \quad (8)$$

where $\phi(E) = 1 - e^{-\left(\frac{E}{\Gamma_i}\right)^2}$ is shape factor [25] responsible for equality $S(E) = 0$ (or $\phi(E) = 0$) at energies $E \leq Q$ i.e. energies lower than reaction threshold.

According to [25] the width was chosen in the form

$$\Gamma(E) = \alpha E^2 + \beta E^3 + \dots \quad (9)$$

In calculating $S(E)$ it suffices to use only the first term of the series with $\alpha \approx \epsilon_F^{-1}$, which effectively takes into account three-quasiparticle configurations. We used the value $\alpha = 0.018 \text{ MeV}^{-1}$, obtained from the averaged experimental widths of GTR resonances. The low-lying discrete states were performed separately.

4 Energies of resonances and charge-exchange strength function for the ^{127}Xe isotope

The calculated charge-exchange strength function $S(E)$ for the ^{127}Xe isotope is shown in Fig. 3 together with experimental data on the $^{127}\text{I}(p, n)^{127}\text{Xe}$ reaction [15]. The strength function $S(E)$ has a resonance character associated with collective excitations of the parent nucleus that receive contributions from various quasiparticle ($p\bar{n}$)-configurations. Of them, dominant ones are determined by $\Delta j = -j_+ - j_-(n-p)$ quasiparticle spin-orbit transitions (spin-flip transitions - *sft*), such as the $1h_{11/2} - 1h_{9/2}(h)$, $2d_{5/2} - 2d_{3/2}(d)$, $1g_{9/2} - 1g_{7/2}(g)$ and to a less extent, by $\Delta j = 0 = j - j$ (core polarization states - *cps*) transitions such as the $1h_{11/2} - 1h_{11/2}(h)$, $2d_{3/2} - 2d_{3/2}(d)$, $1g_{7/2} - 1g_{7/2}$ and $3s_{1/2} - 3s_{1/2}$ transitions. Back-spin-flip quasiparticle excitations with $\Delta j = +1 = j_- - j_+$ (back-spin-flip states - *bsfs*) also contribute: these are $2d_{3/2} - 2d_{5/2}$ and $1g_{7/2} - 1g_{9/2}$ transitions.

Table 1: Contribution (in %) of single-particle ($n-p$) transitions to the structure of charge-exchange excitations of the ^{127}Xe nucleus

Excit. type	E , MeV		Contribution to structure of excitations, %				
	Exper. [15]	Calc. TFFS	$1h_{11/2} - 1h_{9/2}$	$2d_{5/2} - 2d_{3/2}$	$1g_{9/2} - 1g_{7/2}$	$j - j$	$j_- - j_+$
GTR	14.5	14.6	29	12	44	12	3
PR1	8.4	8.3	-	41	33		4
PR2	5.5 - 6.5	6.3	-	-	-	94	6
PR3	3.08	3.1	-	21	6	68	5
	2.62	2.8	-	-	-	96	4
		2.0	-	-	-	13	87

Table 1 presents the contributions of single-particle ($n-p$) transitions into the structure of charge-exchange excitations of ^{127}Xe nucleus both according to experimental data from [15] in the reaction $^{127}\text{I}(p, n)^{127}\text{Xe}$ and according

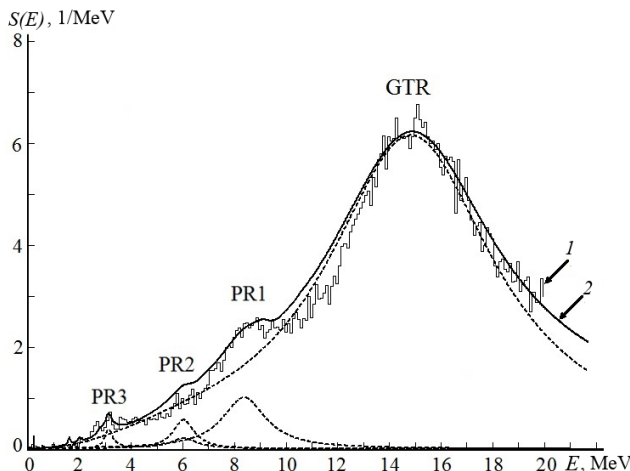


Figure 3: Charge-exchange strength function $S(E)$ of the ^{127}Xe isotope for GT excitations of ^{127}I . Solid line 1 shows experimental data on the $^{127}\text{I}(p, n)^{127}\text{Xe}$ reaction from [15], solid line 2 is our TFFS calculation, and the dashed lines correspond to GTR, PR1, PR2, and PR3 resonances.

to the results of TFFS calculations. The Gamow–Teller resonance (GTR) at 14.6 MeV (the experiment in [15] yields $E_{\text{GTR}}=14.5$ MeV) is the most collective state. Quasiparticle transitions for which $\Delta j = -1 = j_+ - j_-$ make a dominant contribution to the GTR structure (in all, 85%); an excitation formed primarily by spin-flip transitions of the h type lies lower. The calculated PR1 pygmy resonance is close to the respective experimental value; a dominant contribution to its structure comes from spin-flip transitions of the d and g types, and cps transitions of the $j - j$ type also contribute (at a level of 22%). The PR2 pygmy resonance was not found experimentally; theoretically, it is interpreted in terms of two $\Delta j = 0$ cps excitations belonging to the $(j - j)$ type. This means that, according to the terminology adopted in [26], this is a split collective excitation of the ω_0 type. The PR3 resonance is determined by spin-flip transitions of the d type and, primarily, by $\Delta j = 0$ cps transitions. According to calculations, there are two single-particle states at energy range between 2 and 3 MeV: a state at 2.8 MeV determined by $j - j$ transitions of the cps type [that is, $1h_{11/2} - 1h_{11/2}$] and a state at 2.0 MeV determined by $bsfs$ transitions [$2d_{3/2} - 2d_{5/2}$]. States lying below 2 MeV are primarily single-particle states, and we do not consider them in the present study.

Of particular interest are the problem of the sum rule in Eq. (7) and the related *quenching*-effect consisting in the shortage of the sum in Eq. (7) with respect to the maximum theoretical value of $3(N - Z)$ [28] at $q = 1$. The experimental value of the quenching parameter may change greatly from one nucleus to another [10] [21] - for example, from $q = 0.67$ or $67 \pm 8\%$ for ^{98}Mo [29] to $q = 0.85$ or 85% in the case of the ^{127}I nucleus [15].

The integral $I(E_{\text{max}})$ for the isotope ^{127}Xe given by Eq. (7) is shown in Fig. 4 as a function of the energy E_{max} . It is seen that the best description of the experimental data in this case is provided by the calculations with the effective-charge value of $e_q = 0.9$ ($q = 0.81$). The experiment with ^{127}I reported in [15] gives the value $q = 0.85$, close to the calculated value. It is noteworthy that the calculated e_q values for other nuclei differ from 0.9, predominantly on the side of

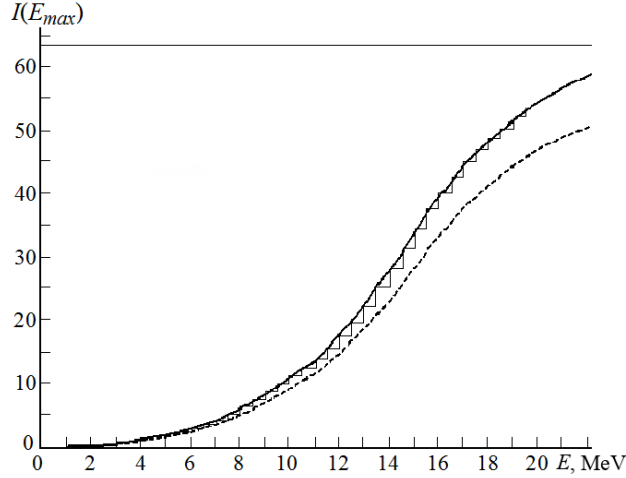


Figure 4: Integral $I(E_{max})$ given by Eq. (7) versus the energy E_{max} for the ^{127}Xe isotope: (steps) experimental data from [15], (solid line) calculation with $e_q = 0.9$, (dashed line) calculation with $e_q = 0.8$, and (horizontal straight line) sum-rule value of $3(N - Z) = 63$.

smaller values [10] [21]. Mostly, this is characteristic of nuclei lighter than ^{127}I and is due partly to the disregard of high-lying (above GTR) excitations in the experiment that are formed by single-particle transitions in which $\Delta n = 1, 2$.

5 Neutrino capture cross-section by the ^{127}I nuclei and Fermi-function

The (ν_e, e^-) cross-section, which depends on the incident-neutrino energy E_ν , has the form [9]:

$$\sigma(E_\nu) = \frac{(G_F g_A)^2}{\pi c^3 \hbar^4} \int_0^{W-Q} W p_e F(Z, A, W) S(x) dx \quad (10)$$

$$W = E_\nu - Q - x - m_e c^2$$

$$c p_e = \sqrt{W^2 - (m_e c^2)^2}$$

where $F(Z, A, W)$ is the Fermi-function, $S(E)$ is the charge-exchange strength function, $G_F/(\hbar c)^3 = 1.1663787(6) \times 10^{-5} \text{ GeV}^{-2}$ is the weak coupling constant and $g_A = -1.2723(23)$ is the axial-vector constant from [30].

Since the change in the Fermi-function according to the Eq. (10) is practically proportional to the change in the cross-section it is essential to allude different approaches how it could be calculated. For more details one could look [31].

General expression for $F(Z, A, W)$ firstly was done into Fermi's paper [32]:

$$F_0(Z, A, W) = 4(2pR)^{2(\gamma-1)} \frac{|\Gamma(\gamma + iy)|^2}{(\Gamma(1 + 2\gamma))^2} e^{\pi y}, \gamma = \sqrt{1 - (\alpha Z)^2}, y = \pm \alpha Z W / p \quad (11)$$

Finite nucleus size can be described by the factor L_0 , such that:

$$F(Z, A, W) = F_0 \cdot L_0.$$

Sufficiently exact expression for L_0 is model dependent. There is a wide use of the Fermi function in which L_0 is obtained by a numerical solution of the Dirac equation [33]:

$$L_0 = 1 \mp \frac{13}{15} \alpha Z W R + \dots \quad (12)$$

More extensive calculations made by Wilkinson [34] gives us next expression for L_0 :

$$L_0 = 1 + \frac{13}{60} (\alpha Z)^2 \mp \frac{\alpha Z W R (41 - 26\gamma)}{[15(2\gamma - 1)]} \mp \frac{\alpha Z R \gamma (17 - 2\gamma)}{[30W(2\gamma - 1)]} + \Omega \quad (13)$$

The correction term Ω is presented in [31]. Papers [35], [36] have importance for nuclei screening estimations and its influence on Fermi-function computation. Fig. 5 demonstrates comparison of few variants of Fermi-functions. It is seen that the greatest differences (up to 15%) are observed at high energies.

The question how to describe and measure the nuclear radius is highly nontrivial. For medium mass isotopes ($A \approx 100$) it is conventional to apply $R = r_0 \cdot A^{1/3} = 1.20 \cdot A^{1/3} \text{ fm}$ formula [37].

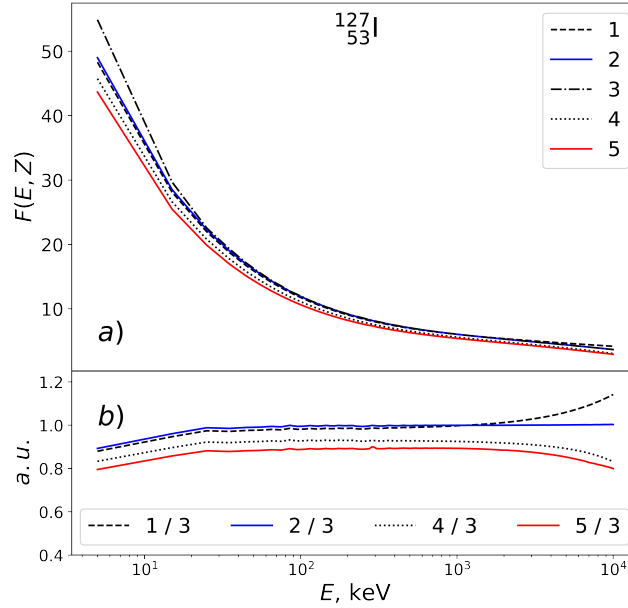


Figure 5: *a)* – Fermi-function calculations: 1 - [32], 2 - [31] with L_0 and spatial charge distribution factors, 3 - [33], 4 - [35], 5 - [36]. *b)* Fermi-functions normalized on [33]. Numbers are the same like in *a)*

Spatial charge distribution $\rho(r)$ could change expression for R . So, departing from uniform distribution, and assuming

$$\rho(r) = \rho_0 \cdot [1 + \exp[(r - R)/a]]^{-1} \quad (14)$$

if $\rho_0 = 0.17 \text{ nucl.} \cdot \text{fm}^{-3}$ и $a = 0.54 \text{ fm}$, we will have [37]:

$$R \approx (1.12 \cdot A^{1/3} - 0.86 \cdot A^{-1/3} + \dots) \text{ fm} \quad (15)$$

More information and an improved $R_C(A)$ dependence and charge distributions for R could be obtained from the analysis of data on analog resonances as in the works [38], [39], [40]. Thus, it was obtained for the charge radius (for nuclei with $A \geq 40$) $R_C = 1.25 \cdot A^{1/3} \text{ fm}$.

Another relation between R and Fermi-function founded by [41] is presented in Bahcall's book (Eq. (8.16) from [42]):

$$R = (2.908 \cdot A^{1/3} + 6.091 \cdot A^{-1/3} - 5.361 \cdot A^{-1}) \cdot 10^{-3} (\hbar/m_e c) \quad (16)$$

After averaging the Fermi-function over the nuclear volume by the radius R , a small correction for the average value (Eq. (8.17) from [42]) will be :

$$\langle F(Z, E) \rangle = [1 - \frac{2}{3}(1 - \gamma)]^{-1} \cdot F(Z, E) \quad (17)$$

Calculation using this Eq. (17) gives a fairly good approximation for the Fermi-function.

Let us note the calculations of the charge radii in the microscopic approach in the framework of the TFFC theory with the Fayans density functional [43]. This calculations were carried out mainly for neutron-deficient spherical nuclei, and the best accuracy was shown for microscopic approaches. For such nuclei, the deviations from the dependence $R \sim A^{1/3}$ are relatively large and approach it near the stability line.

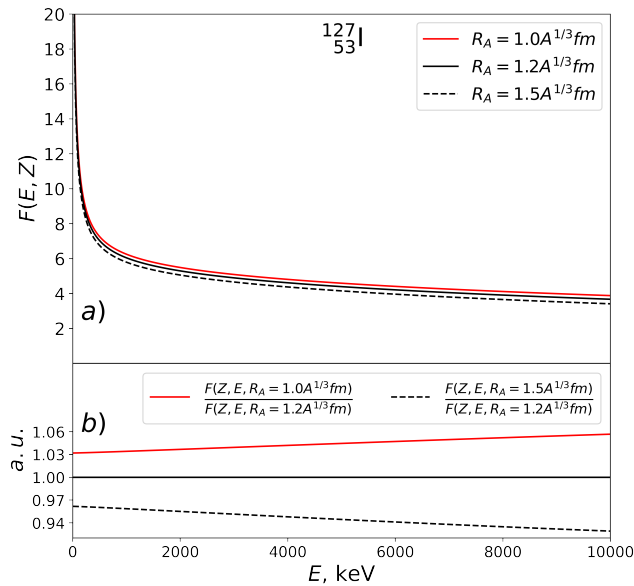


Figure 6: a) Fermi-function [31] with L_0 and spatial charge distribution factors calculated for three values of the parameter r_0 in $R = r_0 \cdot A^{1/3}$: $r_0 = 1.0$, $r_0 = 1.2$ and $r_0 = 1.5$. b) - their ratios.

The isotopic dependence of the charge radii in a long chain of copper isotopes [44] was recently investigated. The same approach was used as in the work [43]: the self-consistent TFFC with the Fayans density functional. Systematic deviation from the $R \sim A^{1/3}$ dependence was observed towards a decrease with increasing neutron excess. Analysis of the experimental data used in [44] showed that for neutron-deficient copper isotopes the deviations from the dependence

$R = 0.96 \cdot A^{1/3} fm$ are $\delta R \approx -2.2\%$ (^{58}Cu), and for neutron-abundant nuclei $\delta R \approx +3.1\%$ (^{78}Cu). Note that in the region of stable nuclei the deviations are insignificant ($\delta R \approx 1.0\%$). Even-odd oscillations are also observed, which depend on the shell structure.

Calculations using the density functional were carried out recently for chains of potassium isotopes ($^{36-52}K$, $Z = 19$) and more heavier nuclei Ca, Sn, Pb [45]. So for isotopes $^{36-52}K$ [46] the fitting gives deviations from the dependence $R = 0.98 \cdot A^{1/3} fm$, $\delta R \leq \pm 4.0\%$, for $^{108-134}Sn$ [47] isotopes $R = 0.94 \cdot A^{1/3} fm$, $\delta R \leq \pm 2.0\%$.

How important is the dependence of the Fermi-function on the radius can be seen from Fig. 6. So with an increase in the parameter r_0 by 25 % from 1.2 to 1.5, the value of the Fermi-function decreases linearly by 4 % at energy $E = 10$ MeV. For the ^{127}I isotope itself, theoretical estimates of the nucleus parameters still require special calculations; nevertheless, the characteristic values for heavy nuclei can be estimated as in [31].

6 Effect of charge-exchange resonances on the neutrino capture cross-section of the ^{127}I nucleus

The cross-sections $\sigma(E)$ for neutrino capture by ^{127}I nuclei in the reaction $^{127}I(\nu_e, e^-)^{127}Xe$ (Fig. 7 and Fig. 8) were calculated with the experimental charge-exchange strength functions $S(E)$ (see Figs. 2 and 3) and with the strength functions $S(E)$ (see Fig. 3) calculated within the TFFS framework according to the method used in [10]. In order to analyze the effect of charge-exchange resonances on the cross-section $\sigma(E)$, we have also performed calculations without taking into account GTR and pygmy resonances.

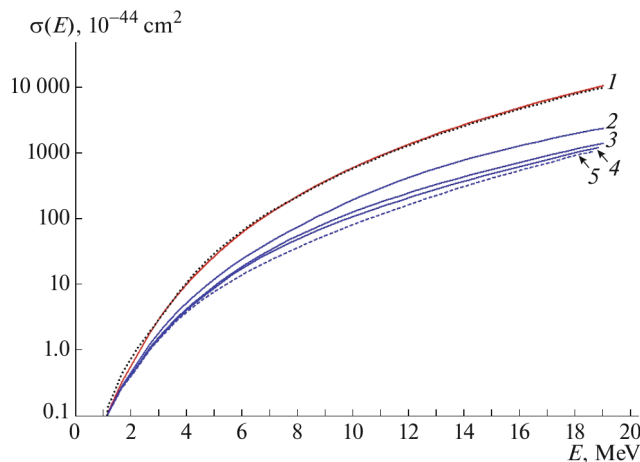


Figure 7: Neutrino-capture cross-section $\sigma(E)$ in the reaction $^{127}I(\nu_e, e^-)^{127}Xe$. The points on display stand for the results of the calculations with the experimental strength function $S(E)$ (see Fig. 2). The solid and dashed curves represent the results of the calculations performed with the strength function $S(E)$ obtained within the TFFS approach (see Fig. 3): (1) summed cross-section; (2) cross-section calculated without GTR; (3) cross-section calculated without GTR and PR1; (4) cross-section calculated without GTR, PR1, and PR2; and (5) cross-section calculated without GTR, PR1, PR2, and PR3

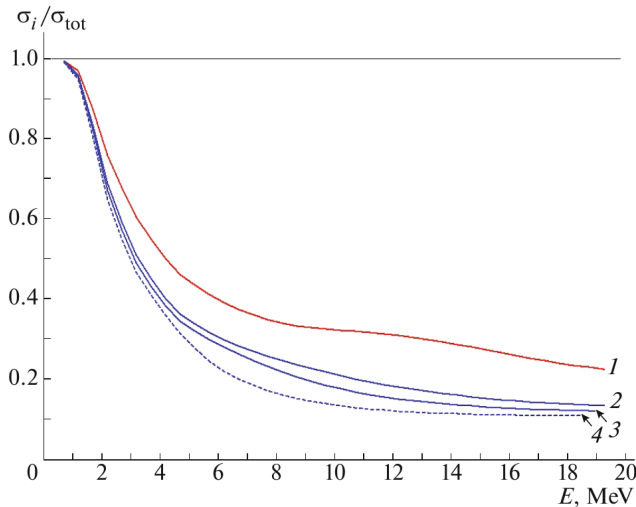


Figure 8: Ratios of the cross-sections $\sigma_i(E)$ calculated for the reaction $^{127}\text{I}(\nu_e, e^-)^{127}\text{Xe}$ and normalized to the summed cross-section $\sigma_{tot}(E)$ determined within the TFFS approach: (1) results calculated without GTR; (2) results calculated without GTR and PR1; (3) results calculated without GTR, PR1, and PR2; and (4) results calculated without GTR, PR1, PR2, and PR3.

Maximum deviation of 30% to 15% from the cross-section summed over all resonances is observed at energies between 1.5 and 2.5 MeV. At energies above 6 MeV, the discrepancies do not exceed 10%. The disregard of only two resonances, GTR and PR1, reduces the cross-section by about 25% to about 80% as the neutrino energy changes from 2 to 12 MeV. It can be seen more clearly in Fig. 8, which shows the ratios of the cross-sections $\sigma_i(E)$ calculated for the reaction $^{127}\text{I}(\nu_e, e^-)^{127}\text{Xe}$ and normalized to the summed cross-section $\sigma_{tot}(E)$ determined within the TFFS approach. Contribution from AR resonance to $\sigma(E)$ is negligible (less than 1%) for the reaction $^{127}\text{I}(\nu_e, e^-)^{127}\text{Xe}$.

7 Solar neutrino capture rate by the ^{127}I nucleus

In order to calculate capture cross-sections for solar neutrinos and to analyze the effect of charge-exchange resonances, it is important to simulate correctly the flux of solar neutrinos. At the present time, there are many models of the Sun. They differ from one another in the relative concentration of helium and elements heavier than helium (metallicity) or may differ in the concentration of some specific element in some part of the Sun (at the center or at the surface). Also, the size of the Sun's convective zone and parameters of medium non-transparency may be different in different models. The BS05(OP), BS05(AGS, OP), and BS05(AGS, OPAL) models developed by the group headed by Bahcall [48] are the most popular models at the present time. There are newer models as well developed by another group. They include the B16-GS98 and B16-AGSS09met models [49] and other. Although B16 models are newer than BS05(OP) models and also agree fairly well with observational data, we present here only BS05(OP) data. Since all known models differ only in the normalization of neutrino fluxes from each nuclear reaction in the Sun, one can readily rescale the data to another model.

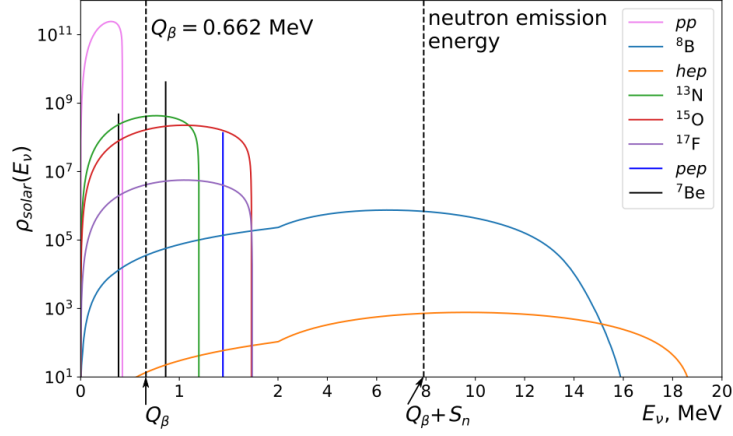


Figure 9: The spectrum of solar neutrinos from [48]. The values of $\rho_{solar}(E_\nu)$ are given in $cm^{-2} \cdot s^{-1} \cdot MeV^{-1}$ (for pep and 7Be lines in $cm^{-2} \cdot s^{-1}$). The threshold energy Q_β of the reaction ${}^{127}I(\nu_e, e^-){}^{127}Xe$ and neutron emission energy $Q_\beta + S_n$ of the ${}^{127}Xe$ nucleus are shown. Please note that the scale changes from 2 MeV. $S_n = 7.246$ MeV, $Q_\beta = 0.662$ MeV.

Figure 9 shows the spectrum of solar neutrinos according to BS05(OP) model [48]. The threshold energy $Q_\beta = 662.3 \pm 2.0$ keV of the reaction ${}^{127}I(\nu_e, e^-){}^{127}Xe$ and neutron separation energy $S_n = 7246 \pm 5$ keV [23] of the nucleus ${}^{127}Xe$ are also shown. It can be seen that, because of the relatively large value of the energy Q_β the intense pp neutrinos (reaction $p + p \rightarrow {}^2H + \nu_e$) with energies $E(\nu) \leq 0.420$ MeV do not contribute to the total capture neutrino spectrum. Note also that, as can be seen from Figs. 2 and 3, most of the strength function $S(E)$ of the ${}^{127}Xe$ isotope is located above the energy 1.74 MeV (maximum energy of the CNO neutrinos of the solar cycle), limiting the most intense part of the solar spectrum. The hep neutrinos (reaction ${}^3He + p \rightarrow {}^4He + e^+ + \nu_e$) and boron neutrinos (reaction ${}^8B \rightarrow {}^8Be^* + e^+ + \nu_e$) could excite the target nuclei to energies corresponding to the resonant part of the strength function $S(E)$ increasing the neutrino capture cross-section.

The neutrino-capture rate R (the number of absorbed neutrinos per unit time) relates to the solar neutrino flux and the capture cross-section by the equation

$$R = \int_0^{E_{max}} \rho_{solar}(E_\nu) \sigma_{total}(E_\nu) dE_\nu \quad (18)$$

where, $E_{max} = 16.36$ MeV for boron neutrinos and $E_{max} = 18.79$ MeV for hep ones [48].

The solar-neutrino capture rate is presented in SNU (1×10^{-36} interactions per target atom per second).

The numerical values of solar-neutrino capture rates R calculated for the reaction ${}^{127}I(\nu_e, e^-){}^{127}Xe$ are given in Table 2 (in SNU). The calculations were made in two assumptions with and without neutron emission process. Excited states with energies higher than $S_n = 7246 \pm 5$ keV [23] decay via neutron emission, whereby the isotope ${}^{126}Xe$ is produced. Difference between this two cases is about 15% to the neutrino capture rate (in **Total**).

For 8B $\sigma_{total} = 4.17/4.99 \times 10^{-42} cm^{-2}$ (with/without neutron emission) is close to the experimental result $(4.3 \pm 0.6) \times 10^{-42} cm^{-2}$ from [15]. Our value

Table 2: Solar-neutrino capture rates R (in SNU) for the isotope ^{127}I with fitted experimental strength function (Fig. 2). The **R -total** was calculated by using the Fermi-function [36] in two assumptions: with and without neutron emission process in the ^{127}Xe nucleus. For each one the result of exclusion GTR and GTR+PR1 from $S(E)$ is shown.

Rate of neutrino capture without neutron emission from the ^{127}Xe nucleus							
	^8B	hep	^{13}N	^{15}O	^{17}F	^7Be	Total
R-total	28.426	0.170	0.148	0.458	0.012	2.656	32.532
R without GTR	8.339	0.039	0.146	0.430	0.011	2.640	12.218
R without GTR and PR1	5.060	0.016	0.145	0.417	0.011	2.631	8.870
Rate of neutrino capture with neutron emission from the ^{127}Xe nucleus							
R-total	23.730	0.096	0.148	0.458	0.012	2.656	27.762
R without GTR	8.339	0.039	0.146	0.430	0.011	2.640	12.218
R without GTR and PR1	5.054	0.016	0.145	0.417	0.011	2.631	8.864

of σ_{Be} is underestimated because of low accuracy of the experimental data at low energies and methodological difficulties in determination of discrete levels width.

The data in Table 2 (see also Figs. 7 and 8) shows that the disregard of even GTR leads to a strong reduction of the cross-section and capture rate (approximately by 70%) in both calculation modes (with/without neutron emission). Fitting resonances with a Gaussian distribution somewhat redistributes the ratio and strength functions $S_i(E)$ of the contributions of the GTR and pygmy resonances to the cross section, without changing the integral effect from all excitations. At solar-neutrino energies upper than S_n , the number of ^{126}Xe atoms arises. The relative amount could be used as an indicator of the presence of hard boron neutrinos in the solar spectrum. From Table 2, one can see the amount of the isotope ^{126}Xe with respect to ^{127}Xe should be about $\approx 15\%$. This is of interest for future experiments with a iodine detector, the more so as ^{126}Xe is a stable isotope released in the form of a gas.

Unfortunately, the accuracy of the experimental strength function measured in known (p, n) reaction is insufficient to correctly discuss the contribution from beryllium neutrinos. More detailed investigation in $(^3\text{He}, t)$ reaction with high resolution could allow to clearly estimate the influence of the discrete components of solar neutrino spectrum.

8 Conclusions

We have studied the effect of high-lying resonances in the nuclear strength function $S(E)$ for solar-neutrino capture cross-section by ^{127}Xe nuclei, performing an analysis of available experimental data from the reaction $^{127}\text{I}(p, n)^{127}\text{Xe}$ [15]. The new values of the charge-exchange resonances energies are slightly different from those obtained earlier.

On the basis of the self-consistent theory of finite Fermi systems, we have calculated the strength function $S(E)$, including the Gamow-Teller and analog resonances, as well as pygmy resonances, which lie lower. The calculations were performed with the parameters of quasiparticle local nucleon–nucleon interaction that were corrected recently [27].

The results of the calculations for the structure of charge-exchange excitations of the ^{127}Xe nucleus are presented, and the contributions of single-particle $(n - p)$ transitions to the resonance states in question have been found. The

giant Gamow-Teller resonance has been shown to be the most collective state. The comparison of the calculated strength function $S(E)$ with experimental data has demonstrated good agreement both in energies and in resonance peak heights. The sum of the calculated squares of matrix elements for excited states corresponds to the theoretical sum rule with an effective charge of $e_q = 0.9$ or $q = 0.81$. This complies with the observed *quenching*-effect (underestimation in the sum rule) parameter.

We have calculated the capture cross-sections $\sigma(E)$ for solar neutrinos and have shown a strong effect of the resonance structure on the $\sigma(E)$, especially in the region of high energies. Also, we have analyzed the effect of each resonance on the energy dependence $\sigma(E)$. We have found that, in calculating $\sigma(E)$, it is necessary to take into account all charge-exchange resonances in the strength function $S(E)$. The disregard of even the high-lying Gamow-Teller resonance leads to a substantial decrease of up to about 70% in the solar-neutrino capture rate for ^{127}I (with inclusion the neutron separation energy for the ^{127}Xe nucleus) owing primarily to high-energy boron neutrinos. The contribution from AR resonance to $\sigma(E)$ is negligible (less than 1%) for the reaction $^{127}\text{I}(\nu_e, e^-)^{127}\text{Xe}$.

We have shown that the inclusion of neutron emission in the consideration reduces the capture rate R , especially for boron and *hep* neutrinos. For neutrino with energies higher than S_n the isotope ^{126}Xe arises in the detector medium area. The relative amount of ^{126}Xe provides an indicator of the high-energy boron and *hep* neutrinos presence in the solar spectrum. We have shown that the number of atoms ^{126}Xe with respect to ^{127}Xe is not small and should be about 17%.

This is of interest for future experiments with iodine detectors, the more so as ^{126}Xe is a stable isotope released, in this case, in the gas form.

We have investigated the influence of different Fermi-functions to the neutrino capture cross-section $\sigma(E)$. It was shown that different approaches gives variation on $\sigma(E)$ to 15%. Nuclear radius gives additional source of uncertainties in determination of Fermi-function. Latest investigations of copper [44] and potassium [46] isotopes gives uncertainties in $\delta R \leq 4\%$ which provides the same variance in Fermi-function.

Unfortunately, current experimental data for ^{127}I were measured only in the (p, n) reaction. To obtain materially more information, it would be proper to have experimental data on the $(^3\text{He}, t)$ reaction. This allows us to return to the idea of large iodine detectors again and on a new level. An experimental study of this issue will help to determine the neutrino capture cross-section significantly more accurately.

In our calculations, we disregarded the effect of neutrino oscillations. Neutrino oscillations reduce the number of electron neutrinos reaching the Earth because of their transformation into other neutrino flavors. However, it is legitimate to ignore neutrino oscillations in our case, where we analyze relative quantities that demonstrate the effect of resonances.

Thus, the article proposes a new type of detector sensitive to the high-energy part of the solar neutrino spectrum. The convenience of this option could be considered the use of a stable and widespread in nature ^{127}I isotope. Also, the chemical inertness of xenon allows to apply various methods for detecting ^{126}Xe isotopes.

9 Acknowledgments

We are grateful to D.N. Abdurashitov, F.T. Avignone, A.L. Barabanov, I.N. Borzov, J. Engel, V.N. Gavrin, L.V. Inzhechik, V.V.Khrushchev, A.Yu. Lutostansky, W. Nazarewicz, N.B. Shul'gina, M.D. Skorokhvatov, S.V. Tolokonnikov and A.K. Vyborov for stimulating discussions and assistance in the work.

10 Funding

This work was supported in part by the Russian Foundation for Basic Research (project no. 18-02-00670); the Division of Neutrino Processes, National Research Center Kurchatov Institute and by the Ministry of Science and Higher Education of the Russian Federation (5-in-100 Program for the Moscow Institute of Physics and Technology (National Research University)).

References

- ¹B. Pontecorvo, “Report PD-205”, Chalk River Labor. Chalk River (1946).
- ²R. Davis, “Solar neutrinos. II. Experimental”, *Phys. Rev. Lett.* **12**, 303–305 (1964).
- ³V. A. Kuzmin, “Preprint No. 62”, Phys. Inst. Acad. Sci., Moscow (1964).
- ⁴V. Kuzmin, “Neutrino production in the ${}^3\text{He}(p, e+\nu){}^4\text{He}$ reaction in solar interiors”, *Physics Letters* **17**, 27–28 (1965).
- ⁵O. G. Ryazhskaya, “Creation of the FIAN neutrino laboratory and underground laboratories”, *Physics-Uspekhi* **61**, 912–920 (2018).
- ⁶M. Wang, G. Audi, F. G. Kondev, W. Huang, S. Naimi, and X. Xu, “The AME2016 atomic mass evaluation (II). Tables, graphs and references”, *Chinese Physics C* **41**, 030003 (2017).
- ⁷W. C. Haxton, “Radiochemical neutrino detection via ${}^{127}\text{I}(\nu_e, e^-){}^{127}\text{Xe}$ ”, *Phys. Rev. Lett.* **60**, 768–771 (1988).
- ⁸Yu. S. Lutostansky and N. B. Shul'gina, “Preprint INE No. 4876/2”, TsNI-Iatominform, Moscow (1989).
- ⁹Yu. S. Lutostansky and N. B. Shul'gina, “Strength function of ${}^{127}\text{Xe}$ and iodine-xenon neutrino detector”, *Phys. Rev. Lett.* **67**, 430–432 (1991).
- ¹⁰Yu. S. Lutostansky and V. N. Tikhonov, “Resonance Structure of the Charge-Exchange Strength Function and Neutrino-Capture Cross Sections for the Isotopes ${}^{71}\text{Ga}$, ${}^{98}\text{Mo}$, and ${}^{127}\text{I}$ ”, *Physics of Atomic Nuclei* **81**, 540–549 (2018).
- ¹¹J. Engel, P. I. Krastev, and K. Lande, “What can be learned with an iodine solar-neutrino detector?”, *Phys. Rev. C* **51**, 2837–2840 (1995).
- ¹²K. Lande, B. Cleveland, R. Davis, et al., “The Homestake Solar Neutrino Program”, *Nuclear Physics B - Proceedings Supplements* **77**, 13–19 (1999).
- ¹³K. Lande, P. Wildenhain, R. Corey, et al., “Measurements of the ${}^8\text{B}$ and ${}^7\text{Be}$ ν_e fluxes from the sun with a Cerenkov triggered radiochemical neutrino detector”, *Nuclear Physics B - Proceedings Supplements* **91**, Neutrino 2000, 50–57 (2001).

- ¹⁴J. R. Distel, B. T. Cleveland, K. Lande, et al., “Measurement of the cross section for the reaction $^{127}\text{I}(\nu_e, e^-)^{127}\text{Xe}_{\text{boundstates}}$ with neutrinos from the decay of stopped muons”, *Phys. Rev. C* **68**, 054613 (2003).
- ¹⁵M. Palarczyk, J. Rapaport, C. Hautala, et al., “Measurement of Gamow-Teller strength for ^{127}I as a solar neutrino detector”, *Phys. Rev. C* **59**, 500–509 (1999).
- ¹⁶J. Engel, S. Pittel, and P. Vogel, “Response of ^{127}I to solar neutrinos”, *Phys. Rev. Lett.* **67**, 426–429 (1991).
- ¹⁷J. Engel, S. Pittel, and P. Vogel, “Capture of solar and higher-energy neutrinos by ^{127}I ”, *Phys. Rev. C* **50**, 1702–1708 (1994).
- ¹⁸Yu. S. Lutostansky, “Charge-exchange pigmy resonances of tin isotopes”, *JETP Letters* **106**, 7–11 (2017).
- ¹⁹Yu. S. Lutostansky, “Charge-exchange isobaric resonances”, *EPJ Web Conf.* **194**, 02009 (2018).
- ²⁰Yu. S. Lutostansky, “Resonance structure of the charge-exchange strength function”, *Physics of Atomic Nuclei* **82**, 528–536 (2019).
- ²¹Yu. S. Lutostansky, A. Osipenko, and V. Tikhonov, “Cross Sections of Solar Neutrino Capture by Nuclei and Charge-Exchange Resonances”, *Bull. Russ. Acad. Sci. Phys.* **83**, 488–492 (2019).
- ²²Yu. S. Lutostansky, G. A. Koroteev, N. V. Klochkova, A. P. Osipenko, V. N. Tikhonov, and A. N. Fazliakhmetov, “Effect of High-Lying Resonances on Cross Sections for Solar-Neutrino Capture by ^{127}I Nuclei”, *Physics of Atomic Nuclei* **83**, 391–399 (2020).
- ²³<https://www-nds.iaea.org>.
- ²⁴Yu. S. Lutostansky, G. Koroteev, N. Klochkova, A. Osipenko, V. Tikhonov, and A. Fazliakhmetov, “New Capabilities of an Iodine Detector for Solar Neutrinos”, *JETP Lett.* **111**, 603–607 (2020).
- ²⁵A. B. Migdal, *Theory of Finite Fermi Systems and Applications to Atomic Nuclei* (Nauka, Moscow, 1983, 2nd ed.; Interscience, New, York, 1967, transl. 1st ed.).
- ²⁶Yu. S. Lutostansky, “Giant gamow-teller resonance: 40 years after the prediction”, *Physics of Atomic Nuclei* **74**, 1176 (2011).
- ²⁷Yu. S. Lutostansky, “Charge-Exchange Isobaric Resonances and Local-Interaction Parameters”, *Physics of Atomic Nuclei* **83**, 33–38 (2020).
- ²⁸A. Arima, “History of giant resonances and quenching”, *Nuclear Physics A* **649**, Giant Resonances, 260–270 (1999).
- ²⁹J. Rapaport, P. Welch, J. Bahcall, et al., “Solar-Neutrino Detection: Experimental Determination of Gamow-Teller Strengths via the ^{98}Mo and ^{115}In (p, n) Reactions”, *Phys. Rev. Lett.* **54**, 2325–2328 (1985).
- ³⁰P. A. Zyla, R. M. Barnett, J. Beringer, et al., “Review of Particle Physics”, *Progress of Theoretical and Experimental Physics* **2020**, 083C01 (2020).
- ³¹L. Hayen, N. Severijns, K. Bodek, D. Rozpedzik, and X. Mougeot, “High precision analytical description of the allowed β spectrum shape”, *Rev. Mod. Phys.* **90**, 015008 (2018).

- ³²E. Fermi, “An attempt of a theory of beta radiation. 1.”, *Z. Phys.* **88**, 161–177 (1934).
- ³³H. Behrens and J. Jänecke, *Numerical Tables for Beta-Decay and Electron Capture / Numerische Tabellen für Beta-Zerfall und Elektronen-Einfang*, edited by H. Schopper, Vol. 4, Landolt-Boernstein - Group I Elementary Particles, Nuclei and Atoms (Springer, 1969).
- ³⁴D. Wilkinson, “Evaluation of beta-decay: II. Finite mass and size effects”, *Nuclear Instruments and Methods in Physics Research Section A: Accelerators, Spectrometers, Detectors and Associated Equipment* **290**, 509–515 (1990).
- ³⁵B. S. Dzhelepov and L. N. Zyrianova, *Influence of atomic electric fields on beta decay* (Moscow: Akad. Nauk SSSR, 1956).
- ³⁶Y. P. Suslov, *Izv. Akad. Nauk SSSR, Ser. Fiz.* **32**, 213 (1968).
- ³⁷A. Bohr and B. R. Mottelson, *Nuclear Structure V.1* (W. A. Benjamin Inc., 1969).
- ³⁸Yu. S. Lutostansky and V. N. Tikhonov, “Phenomenological description of the Coulomb energies of medium-heavy and superheavy nuclei”, *Bull. Russ. Acad. Sci. Phys.* **79**, 425–430 (2015).
- ³⁹J. D. Anderson, C. Wong, and J. W. McClure, “Coulomb displacement energies derived from the p, n isobaric reaction”, *Phys. Rev.* **138**, B615–B618 (1965).
- ⁴⁰C. Batty, R. Gilmore, and G. Stafford, “Isobaric states excited in (p, n) reactions at 30 and 50 MeV”, *Nuclear Physics* **75**, 599–608 (1966).
- ⁴¹L. R. Elton, *Nuclear sizes* (Clarendon Press, Oxford University Press, London, 1961.).
- ⁴²J. N. Bahcall, *Neutrino Astrophysics* (Cambridge University Press. 1988.).
- ⁴³E. E. Saperstein and S. V. Tolokonnikov, “Self-consistent theory of finite fermi systems and skyrme–hartree–fock method”, *Physics of Atomic Nuclei* **79**, 1030–1066 (2016).
- ⁴⁴I. N. Borzov and S. V. Tolokonnikov, “Self-Consistent Calculation of the Charge Radii in a Long $^{58-82}\text{Cu}$ Isotopic Chain”, *Physics of Atomic Nuclei* **83**, 828–840 (2020).
- ⁴⁵P.-G. Reinhard, W. Nazarewicz, and R. F. Garcia Ruiz, “Beyond the charge radius: the information content of the fourth radial moment”, *Phys. Rev. C* **101**, 021301 (2020).
- ⁴⁶Á. Koszorús, X. F. Yang, W. G. Jiang, et al., “Charge radii of exotic potassium isotopes challenge nuclear theory and the magic character of $N = 32$ ”, *Nature Physics* (2021).
- ⁴⁷C. Gorges, L. V. Rodriguez, D. L. Balabanski, et al., “Laser Spectroscopy of Neutron-Rich Tin Isotopes: A Discontinuity in Charge Radii across the $N = 82$ Shell Closure”, *Phys. Rev. Lett.* **122**, 192502 (2019).
- ⁴⁸J. N. Bahcall, A. M. Serenelli, and S. Basu, “New solar opacities, abundances, helioseismology, and neutrino fluxes”, *The Astrophysical Journal* **621**, L85–L88 (2005).
- ⁴⁹N. Vinyoles, A. M. Serenelli, F. L. Villante, S. Basu, J. Bergström, M. C. Gonzalez-Garcia, M. Maltoni, C. Peña-Garay, and N. Song, “A new generation of standard solar models”, *The Astrophysical Journal* **835**, 202 (2017).